Reduction of C=C Double Bonds by Hydrazine using Active Carbons as Metal-Free Catalysts

Juan Carlos Espinosa,[a] Sergio Navalon,[a] Mercedes Alvaro, [a] Amarajothi Dhakshinamoorthy,*[a,b] Hermenegildo Garcia*[a,c]

[a] Departamento de Química and Instituto Universitario de Tecnología Química Consejo Superior de Investigaciones Científicas-Universitat Politécnica de Valencia, Universitat Politècnica de València, Av. De los Naranjos s/n, 46022, Valencia, Spain.

[b] School of Chemistry, Madurai Kamaraj University, Palkalai Nagar, Madurai 625 021, Tamil Nadu, India. E-mail: admguru@gmail.com

[c] Centre of Excellence for Advanced Materials Research, King Abdulaziz University, Jeddah, Saudi Arabia.

Number of pages: 19

Total figures: 16

Total tables: 4

Contents

Table S1. Elemental analyses (wt %) of AC-6 treated samples.

Catalyst	N	C	H	O
AC-6=NPh	1.89	67.6	1.17	29.34
AC-6_EG	0.83	64.7	1.78	32.69
AC-6_CO_2Me, =NPh	1.38	67.55	1.09	29.98
AC-6_CO_2Me	0.76	66.22	1.23	31.79

Table S2. TPD estimation of density functional groups in the AC-6 treated materials.[a]

Catalyst	% Carboxylic acid (CO_2)	% Lactone (CO_2)	% Anhydride (CO_2+CO)	% Phenol (CO)	% Ether (CO)	% Carbonyl /Quinone (CO)
AC-6=NPh	70.0	30.0	-	-	-	-
AC-6_EG	47. 5	2.0	-	18.3	22.6	9.7
AC-6_CO_2Me, =NPh	-	4.1	44.4	2.7	34.2	14.6
AC-6_CO_2Me	-	23.1	29.0	4.8	28.8	14.4

[a] Estimation has been done considering the area below the TPD curve

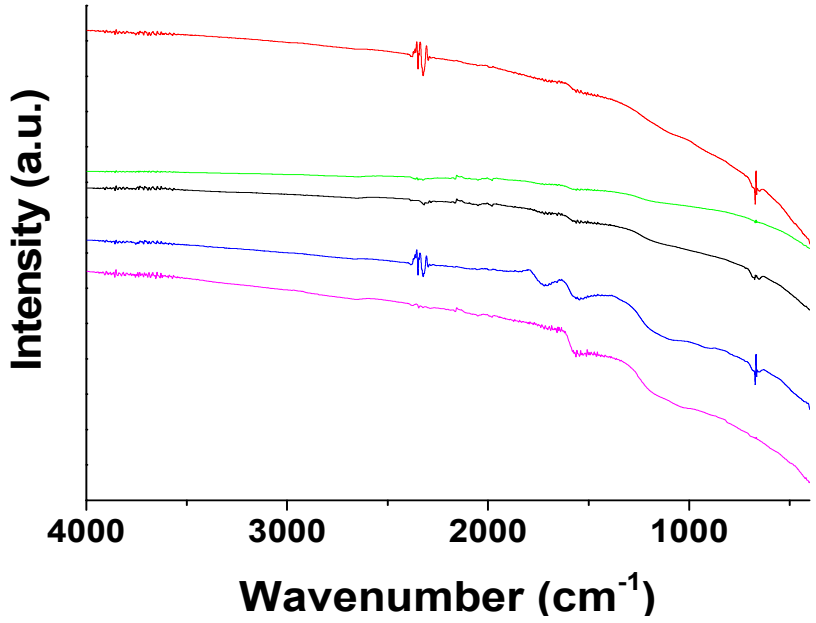

Figure S1. ATR-IR spectra. AC (red), AC-3 (green), AC-6 (black), AC-20 (blue) and AC-6 6 times used (pink).

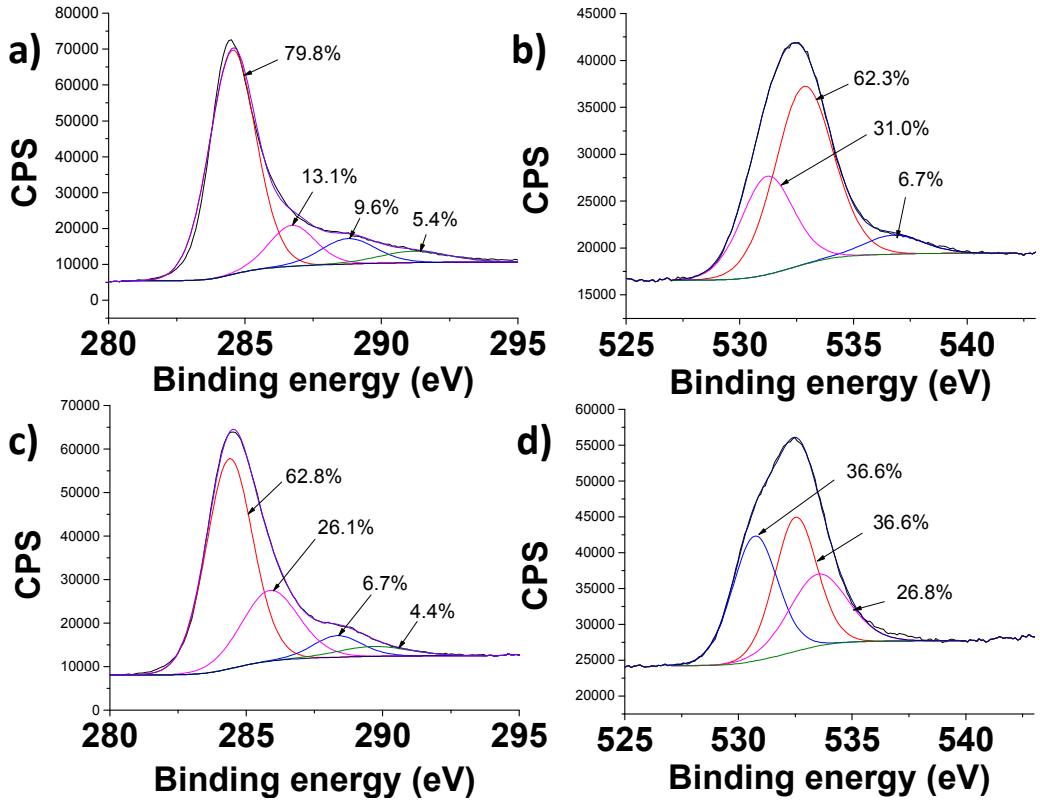

Figure S2. XPS spectra of C1s (a, c) and O1s (b, d) for AC-3 (a, b) and AC-20 (c, d).

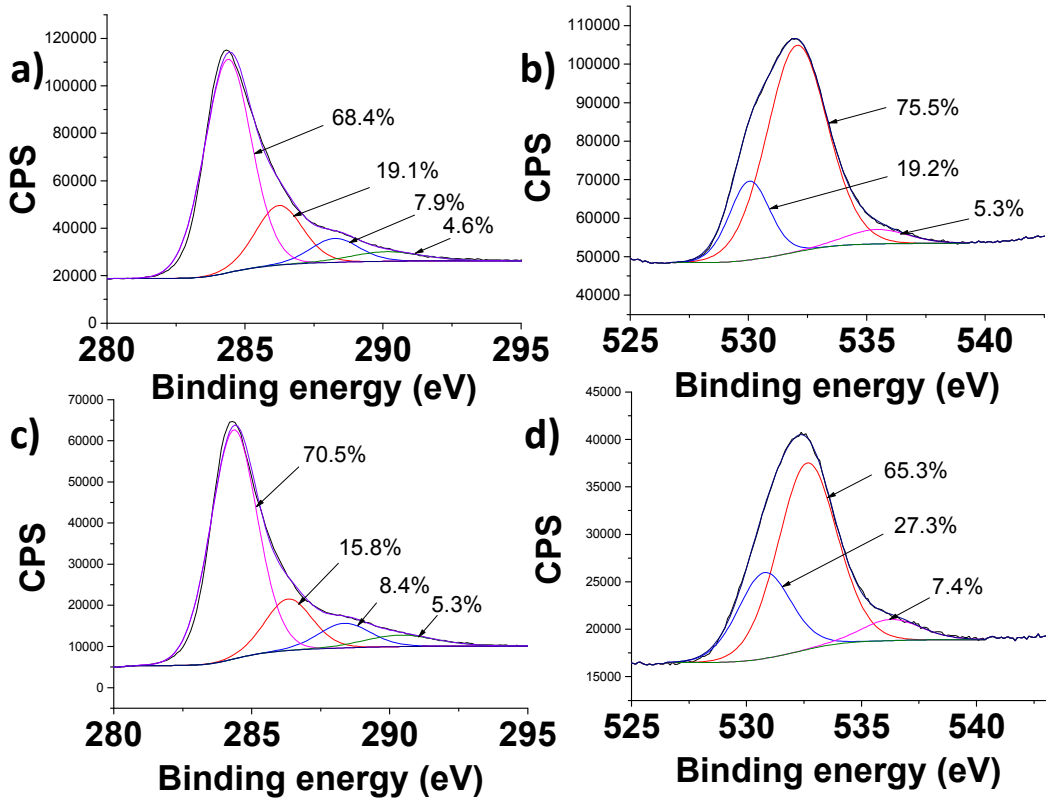

Figure S3. XPS spectra (C1s and O1s) for AC-6 (a, b) and AC-6 six times used (c, d).

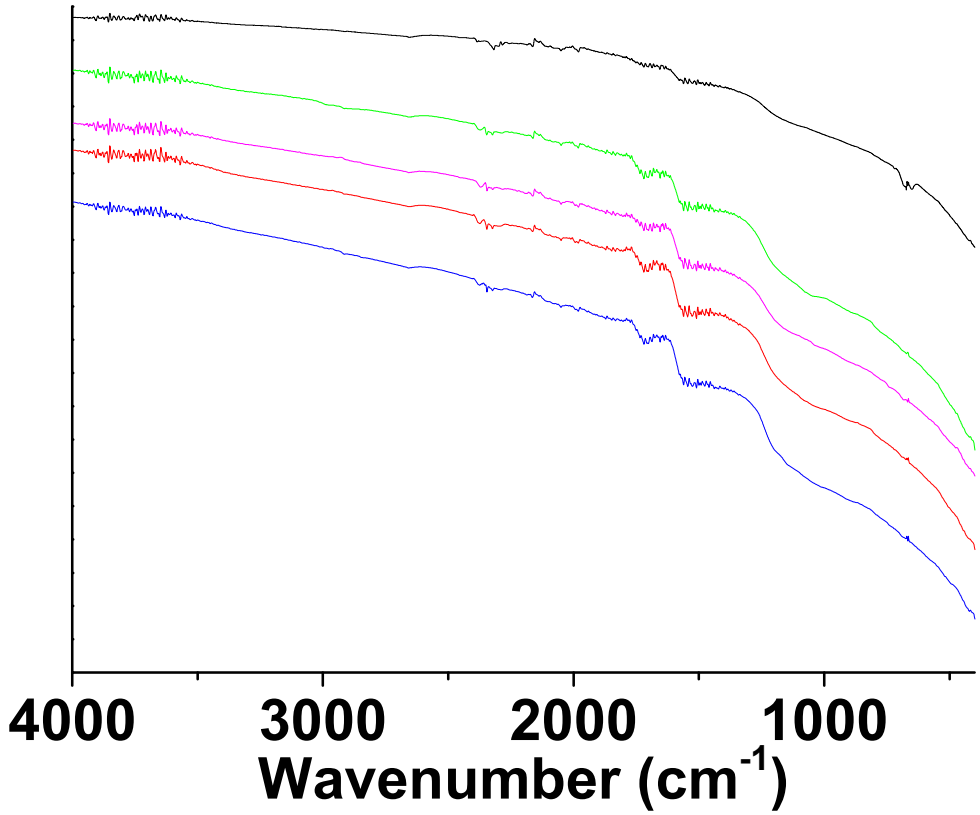

Figure S4. ATR-IR spectra for the AC-6 treated materials. AC-6 (black), AC-6_CO_2Me (green), AC-6=NPh (pink), AC-6_CO_2Me, =NPh (blue), AC-6_EG (red).

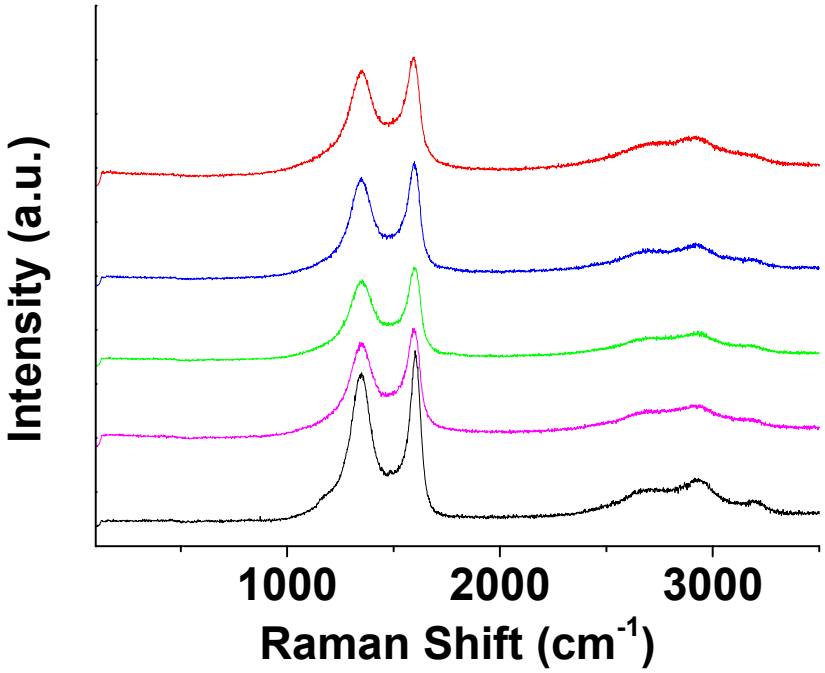

Figure S5. Raman spectra for AC and the AC-6 treated materials. AC-6 (black), AC-6_CO_2Me (green), AC-6=NPh (pink), AC-6_CO_2Me, =NPh (blue), AC-6_EG (red).

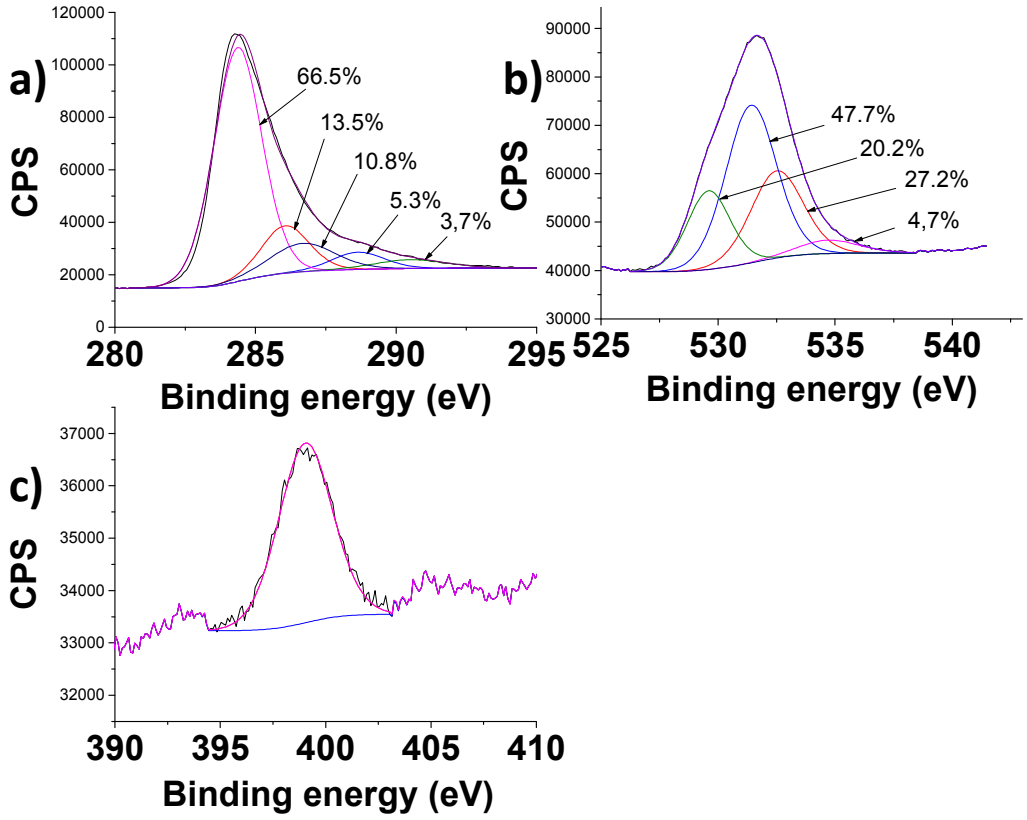

Figure S6. XPS analysis for AC-6=NPh. C1s (a), O1s (b) and N1s (c).

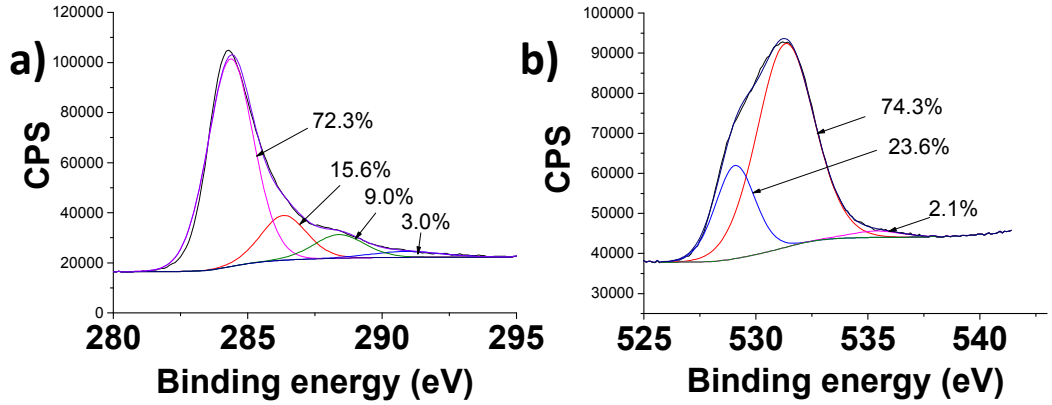

Figure S7. XPS analysis for AC-6_CO_2Me. C1s (a) and O1s (b).

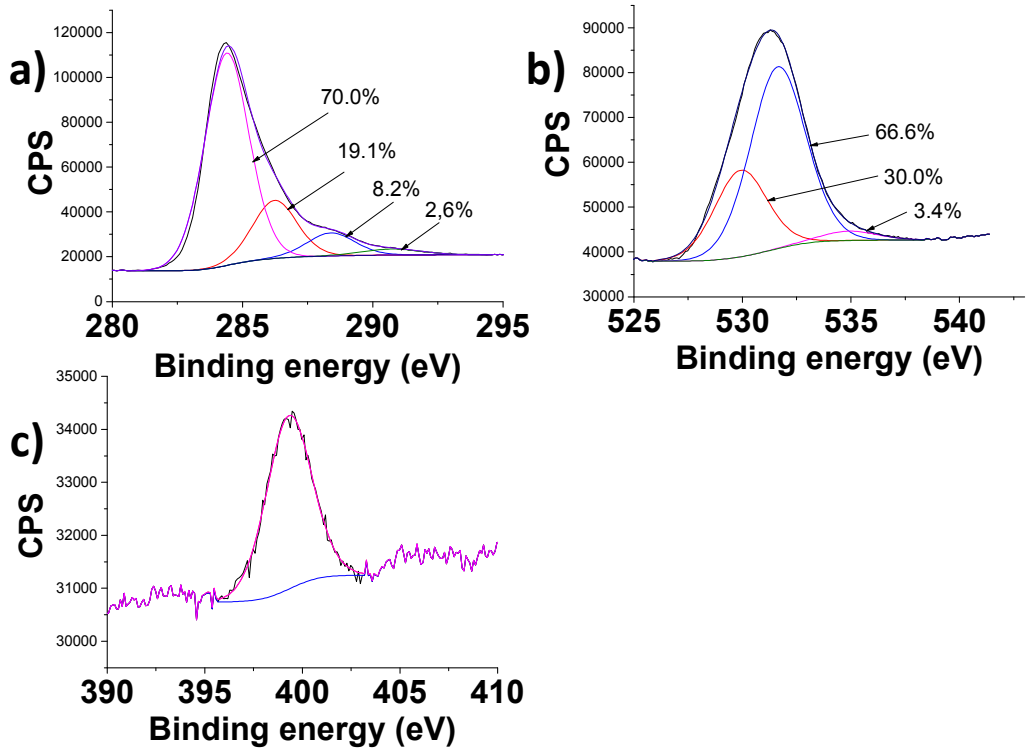

Figure S8. XPS analysis for AC-6_CO_2Me, =NPh. C1s (a), O1s (b) and N1s (c).

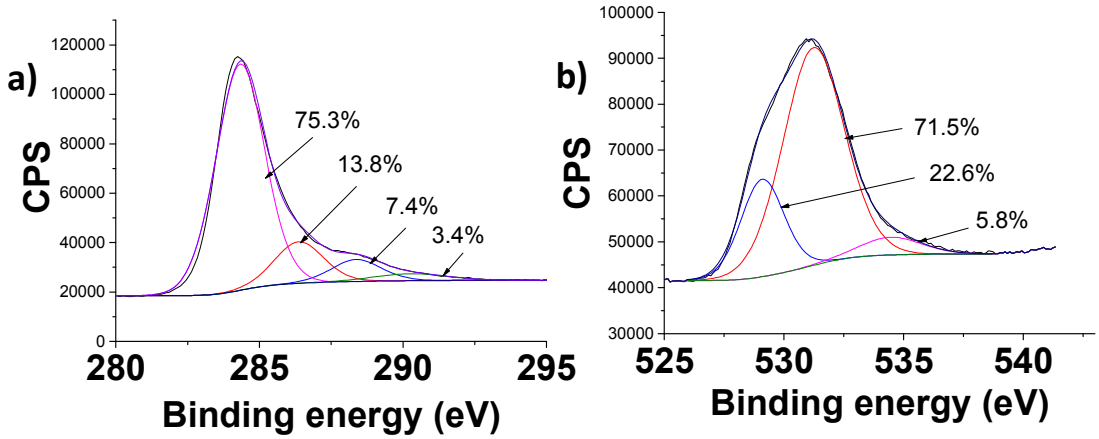

Figure S9. XPS analysis for AC-6_EG. C1s (a) and O1s (b).

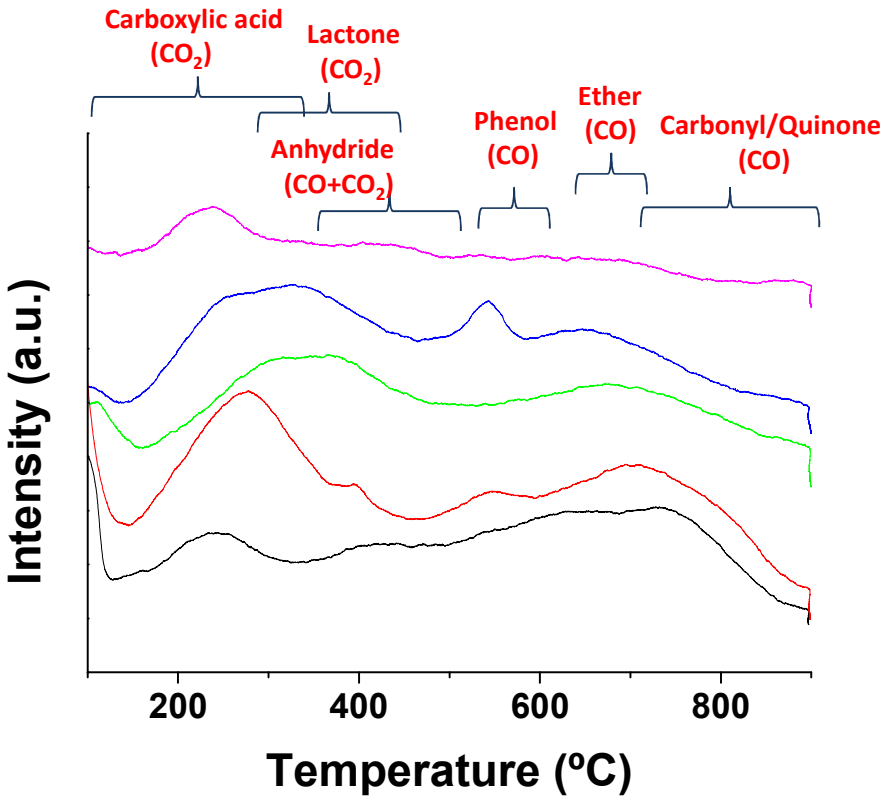

Figure S10. TPD analysis. AC-6 (black), AC-6_CO_2Me (green), AC-6=NPh (pink), AC-6_CO_2Me, =NPh (blue), AC-6_EG (red).

Table S3. Textural properties of various commercial samples employed in this work.[1]		
Support	S_{BET} (m^2/g)	size
Diamond	200-450	< 10 nm
Graphite	47	200-500 nm
MWCNT	200-350	10-20 nm diameter and 10-500 nm length
Graphene	-[a]	Thickness < 1nm, lateral dimensions (~ 1 μm)

[a]Isothermal nitrogen adsorption on dry Graphene powder is not a suitable technique to measure surface area of G dispersed in liquid media.

In addition, we have determined the elemental analysis of commercial graphite, MWCNTs, nanometric diamond and graphene from alginate pyrolyzed at 900 ^{o}C and the observed results are given in Table S4. As expected commercial graphite and MWCNTs are mainly constituted by carbon (> 97 %) and small amounts of oxygen (< 2.6 wt%) and hydrogen (< 0.23 wt%). In the case of commercial diamond nanoparticles carbon (~ 88wt%) is accompanied by significant amounts of oxygen (~ 8 wt%) and nitrogen (~2.5). This composition in commercial diamond nanoparticles is not unexpected considering nanodiamonds are obtained by detonation of explosives such as trinitrotoluene and hexogen substances in a deficient oxygen atmosphere. In the case of graphene from alginate, obtained by pyrolysis of alginate biopolymer, the composition contains mainly carbon atoms (~ 86.4 wt%) with a considerable amount of oxygen (~12.6 wt%) .

Table S4. Elemental analysis (wt %) of samples employed in this work.

	N(%)	**C (%)**	**H (%)**	**O (%)**
G from Alginate	0.35	86.4	0.65	12.6
Graphite	0.00	99.63	0.06	0.31
Diamond NPs	2.46	88.42	0.86	8.26
MWCNTs	0.00	97.14	0.23	2.63

Raman spectroscopy clearly shows the presence of sp^2 hybridized carbons in the commercial graphite, MWCNTs as well as in graphene from alginate characterized by the presence of the so-called G band that appears at about 1583 cm^{-1}. In these three carbonaceous samples the presence of the D band at about 1312 cm^{-1} is also observed. This D band is frequently attributed to the presence of defects or disorder in the carbon structure. As expected commercial nanometric diamond does not exhibit any characteristic peak in Raman spectroscopy.

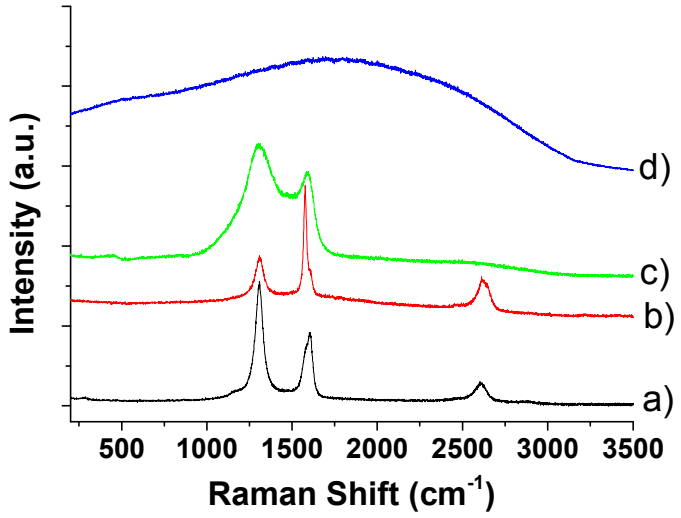

Figure S11. Raman spectra of commercial MWCNTs (a), commercial graphite (b), graphene from alginate (c) and commercial diamond nanoparticles (d).

XPS analysis of commercial graphite, MWCNTs, nanometric diamond and graphene from alginate were also measured. In agreement with the previous comments about commercial MWCNTs and graphite, XPS spectra of both carbonaceous materials (Figures S12-13) show that the main band corresponds to C=C bonds with small contributions of oxygen-functional groups. In the case of graphene from alginate (Figure S14), deconvolution of the C 1s peak shows a main contribution of the C sp^2 atoms, accompanied by C atoms bonded to such as C-O, C=O and O-C=O. In the case of commercial diamond nanoparticles (Figure S15) the C 1s band deconvolution shows the presence of two main components that can be attributed to the presence of sp^3 and sp^2 carbons. The presence of sp^2 carbons in commercial diamond nanoparticles has been previously established as C atoms of amorphous material embedding the well crystallized sp^3 nanometric diamond. It should be noted, however, that XPS is a surface technique that in the case of diamond nanoparticles overestimates the presence of sp^2 carbons respect to the bulk material.

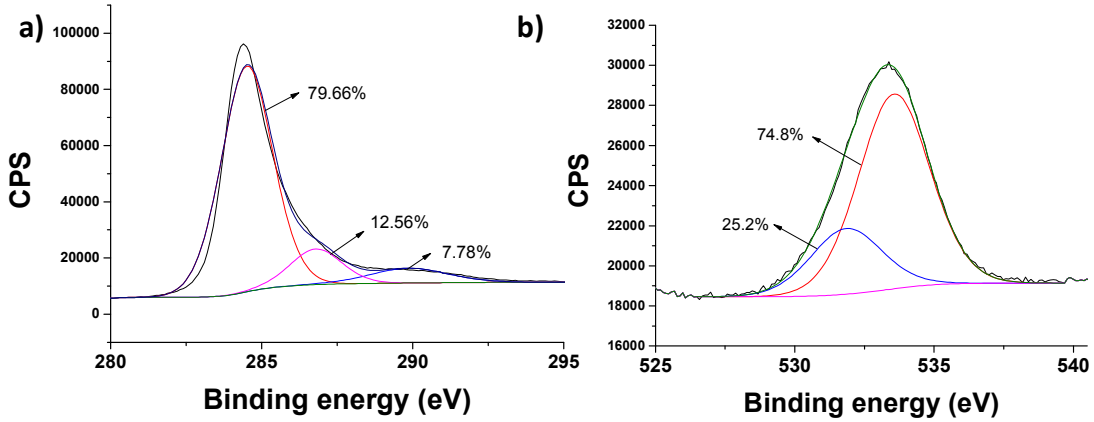

Figure S12. High-resolution XPS of C 1s (a) and O 1s (b) peaks measured for commercial MWCNTs. Best deconvolution curve and its atomic percentage are indicated. Atomic concentrations: C (93.71 at.%) and O (6.29 at.%) .

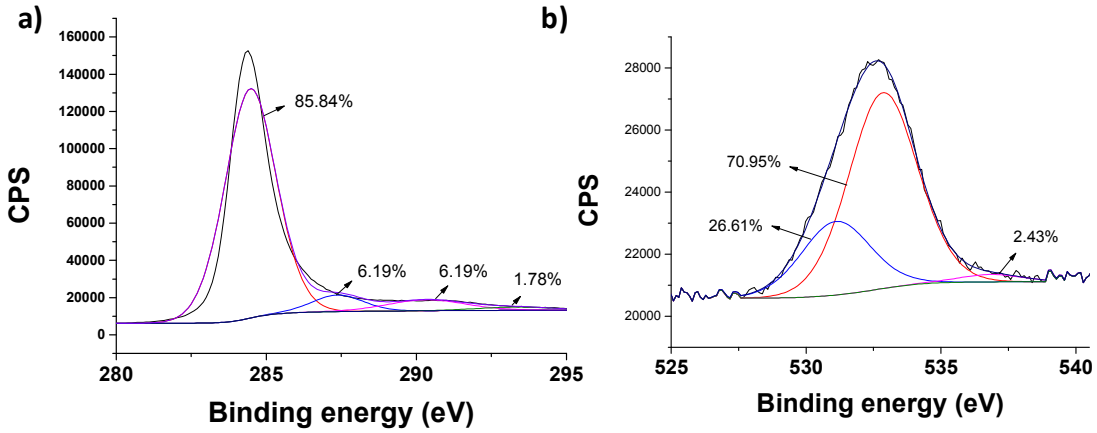

Figure S13. High-resolution XPS of C 1s (a) and O 1s (b) peaks measured for commercial graphite. Best deconvolution curve and its atomic percentage are indicated. Atomic concentrations: C (96.34 at.%) and O (3.66 at.%).

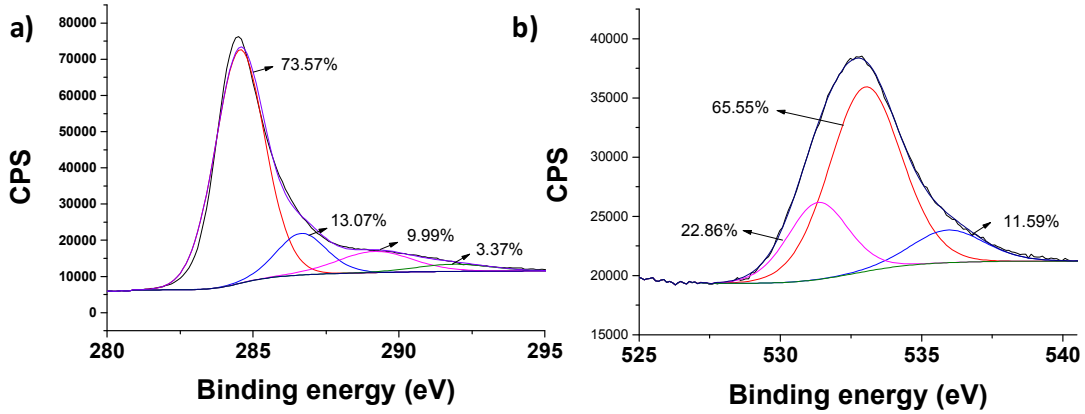

Figure S14. High-resolution XPS of C 1s (a) and O 1s (b) peaks measured for graphene from Alginate. Best deconvolution curve and its atomic percentage is indicated. Atomic concentrations: C (87.79 at.%) and O (12.21 at.%).

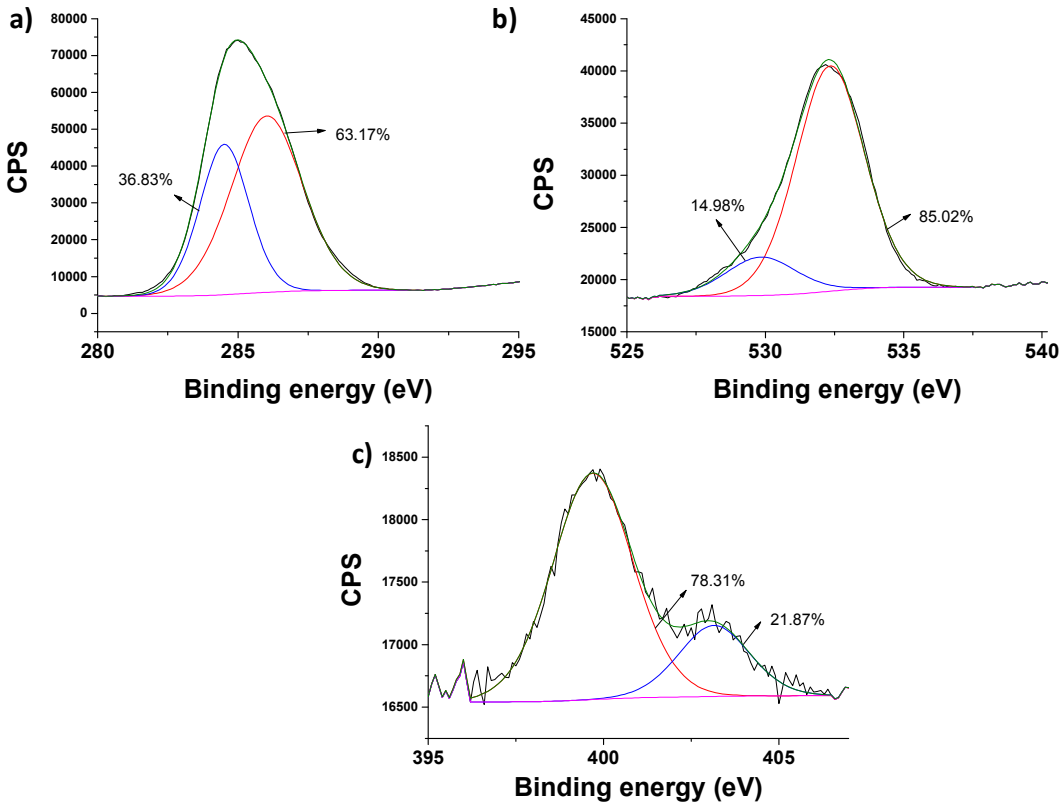

Figure S15. High-resolution XPS of C 1s (a), O 1s (b) and N 1s (c) peaks measured for commercial diamond nanoparticles. Best deconvolution curve and its atomic percentage are indicated. Atomic concentrations: C (89.05 at.%), O (9.61 at.%) and N (1.34 at.%).

Commercial AC, AC-3, AC-6 and AC-20 were also characterized by recording the zeta potential of carbonaceous aqueous suspensions at different pH values. Figure S16 shows that the lower zeta potential value in the entire pH region as well as the lower isoelectric point decreases as the carbon surface oxidation increases. Furthermore, the resulting pH of an aqueous suspension of carbonaceous samples (5 mg ml^{-1}) employed in this work also decreases as the carbon surface oxidation increases: AC (pH 5.72), AC-3 (pH 3.78), AC-6 (pH 3.72) and AC-20 (pH 3.44). These observations are in agreement with the deeper carbon surface oxidation and the presence of higher densities of acidic oxygen functionalities as the strength of oxidation increases.

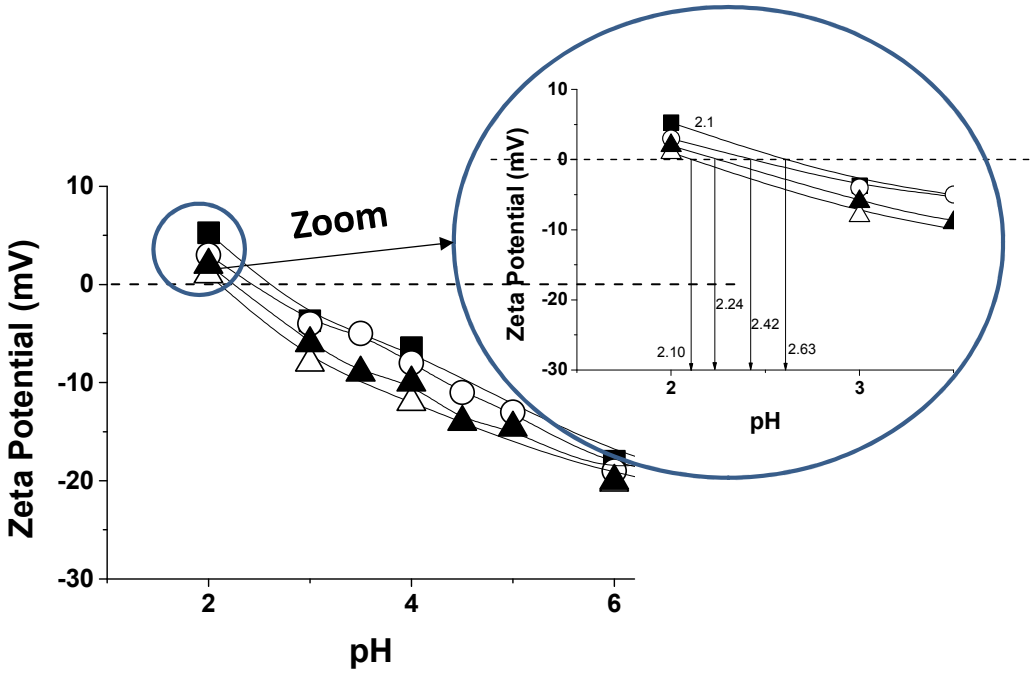

Figure S16. Zeta potential values in the entire pH region for AC-3, AC-6 and AC-20 samples.

References

1. Dhakshinamoorthy, A.; Navalon, S.; Sempere, D.; Alvaro, M.; Garcia, H., Chem. Commun., 2013,49, 2359-2361.